MAEL contributes to gastric cancer progression by promoting ILKAP degradation

SUPPLEMENTARY MATERIALS

Supplementary Table 1: Antibodies used in the study

Antibodies against	Catalog No	Source
MAEL	PA5-20923	ThermoFisher, Rockford, IL, USA
ILKAP	HPA004752	Sigma-Aldrich, St.Louis, MO, USA
ILKAP	H00080895-B01P	Novus Biologicals, Littleton, CO, USA
p38 MAPK	8690	CST, Danvers, MA, USA
phospho-p38 (T180/T182)	4511	CST, Danvers, MA, USA
phospho-RSK2 (S227)	3556	CST, Danvers, MA, USA
phospho-Chk1(S345)	2348	CST, Danvers, MA, USA
Phospho-GSK-3β (S9)	5558	CST, Danvers, MA, USA
Phospho-Akt (S473)	4060	CST, Danvers, MA, USA
E-cadherin	3195	CST, Danvers, MA, USA
N-cadherin	13116	CST, Danvers, MA, USA
β-Actin	AT0001	CMCTAG, Milwaukee, WI, USA
GAPDH	AT0002	CMCTAG, Milwaukee, WI, USA
Myc-tag	C3956	Sigma-Aldrich, St.Louis, MO, USA
HA-tag	SAB1305536	Sigma-Aldrich, St.Louis, MO, USA
HRP-labeled goat α-rabbit IgG	074-1506	KPL, Gaithersburg, MD, USA
HRP-labeled goat α-mouse IgG	5220-0287	KPL, Gaithersburg, MD, USA

Supplementary Table 2: Chemicals used in the study

Chemicals	Source
hygromycin B	BBI, Shanghai, China
puromycin	BBI, Shanghai, China
Leupetin	BBI, Shanghai, China
Chloroquine	BBI, Shanghai, China
MG132	BBI, Shanghai, China
3-MA	BBI, Shanghai, China
5-aza-2-deoxycytidine	Sigma-Aldrich, St.Louis, MO, USA
MTT	BBI, Shanghai, China

Supplementary Table 3: The clinicopathological parameters of the gastric cancer patients used in the study

Gender	Age	Pathology	Differentiation	Diameter	TNM	Stage
Male	86	adenocarcinoma	poor	4 cm	T3N1M1	III
Male	55	adenocarcinoma	high	1 cm	T1N0M0	I
Female	48	adenocarcinoma	poor	2.5 cm	T3N0M0	II
Male	68	adenocarcinoma	poor	4 cm	T3N0M1	II

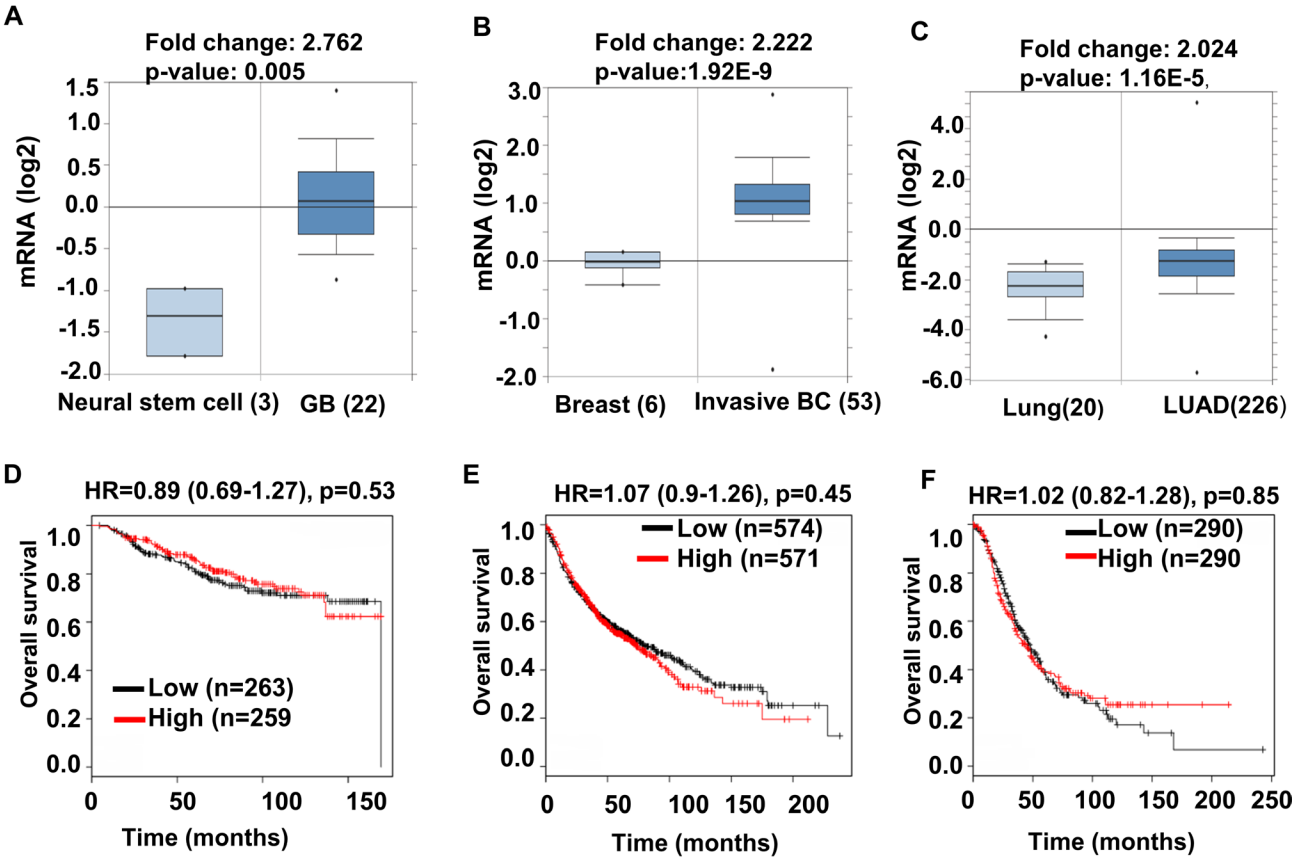

Supplementary Figure 1: Expression and prognostic significance of *MAEL* gene. (**A**–**C**) Differential expression of *MAEL* mRNA in normal and cancer tissues were analyzed using Onocomine based on the NCBI GEO datasets (glioblastoma: GSE4536, invasive breast cancer: GSE9014 and lung adenocarcinoma: GSE31210). GB: glioblastoma, BS: breast cancer, OS: overall survival, LUAD: lung adenocarcinoma. (**D**–**F**) The survival curves of patients with breast (**D**), lung (**E**) and ovarian (**F**) cancers were plotted using Kaplan Meier plotter, which includes 5,143 breast, 1,816 ovarian, 2,437 lung and 1,065 gastric cancer patients with a mean follow-up of 69/40/49/33 months.

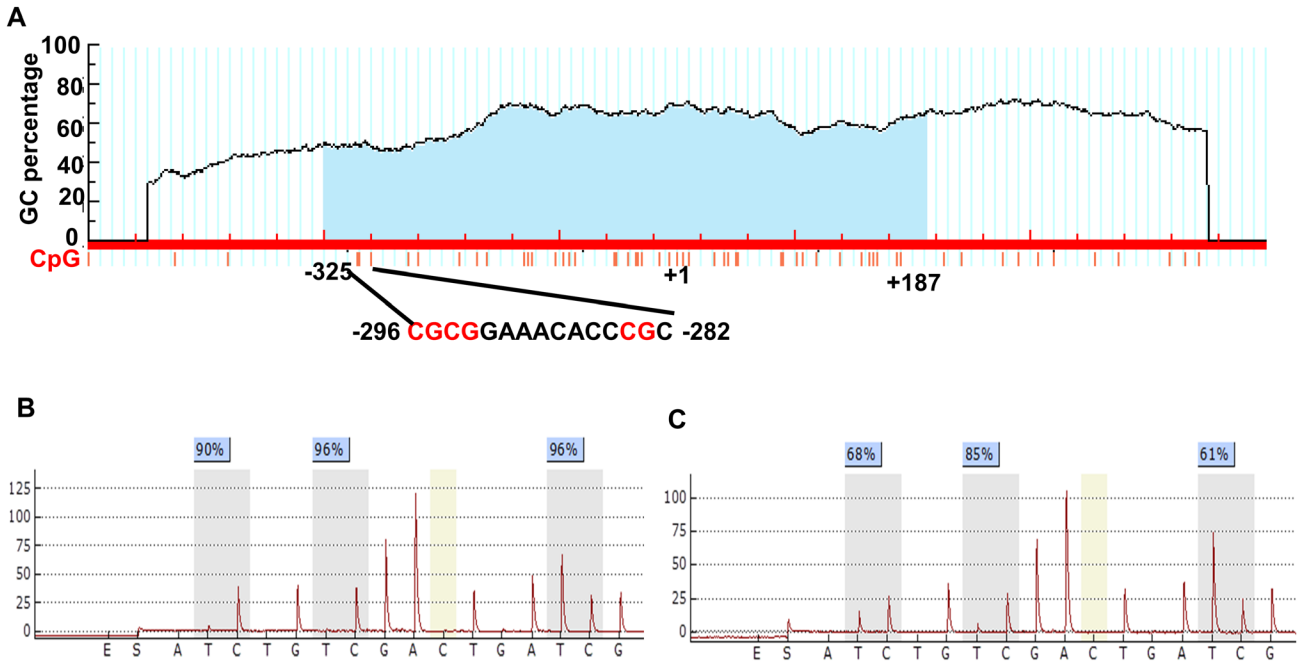

Supplementary Figure 2: Methylation level of *MAEL* gene promoter was quantified by pyrosequencing. (**A**) Schematic diagram of the *MAEL* gene promoter. The CpG island (blue) was predicted by MethPrimer software, which locates at nucleotides −293 to +178, relative to transcription start site (+1). The sequence to be detected by pyrosequencing is CGCGGAAACACCCGC, which includes 3 CpG dinucleotides. (**B**, **C**) The pyrograms of an adjacent normal gastric tissue (**B**) and a gastric tumor tissue (**C**). Grey areas indicate the CpG sites that were analyzed. The percentages (blue) are the proportion of C at each CpG site after bisulfite conversion. The yellow regions indicate controls regions for automatic assessment of bisulfite conversion (unmethylated C should be fully converted to T). An overall *MAEL* promoter methylation level is calculated as the average of the proportions of C (%) at the 3 CpG sites. The y-axis represents the signal intensity, the x-axis shows the dispensation sequence.

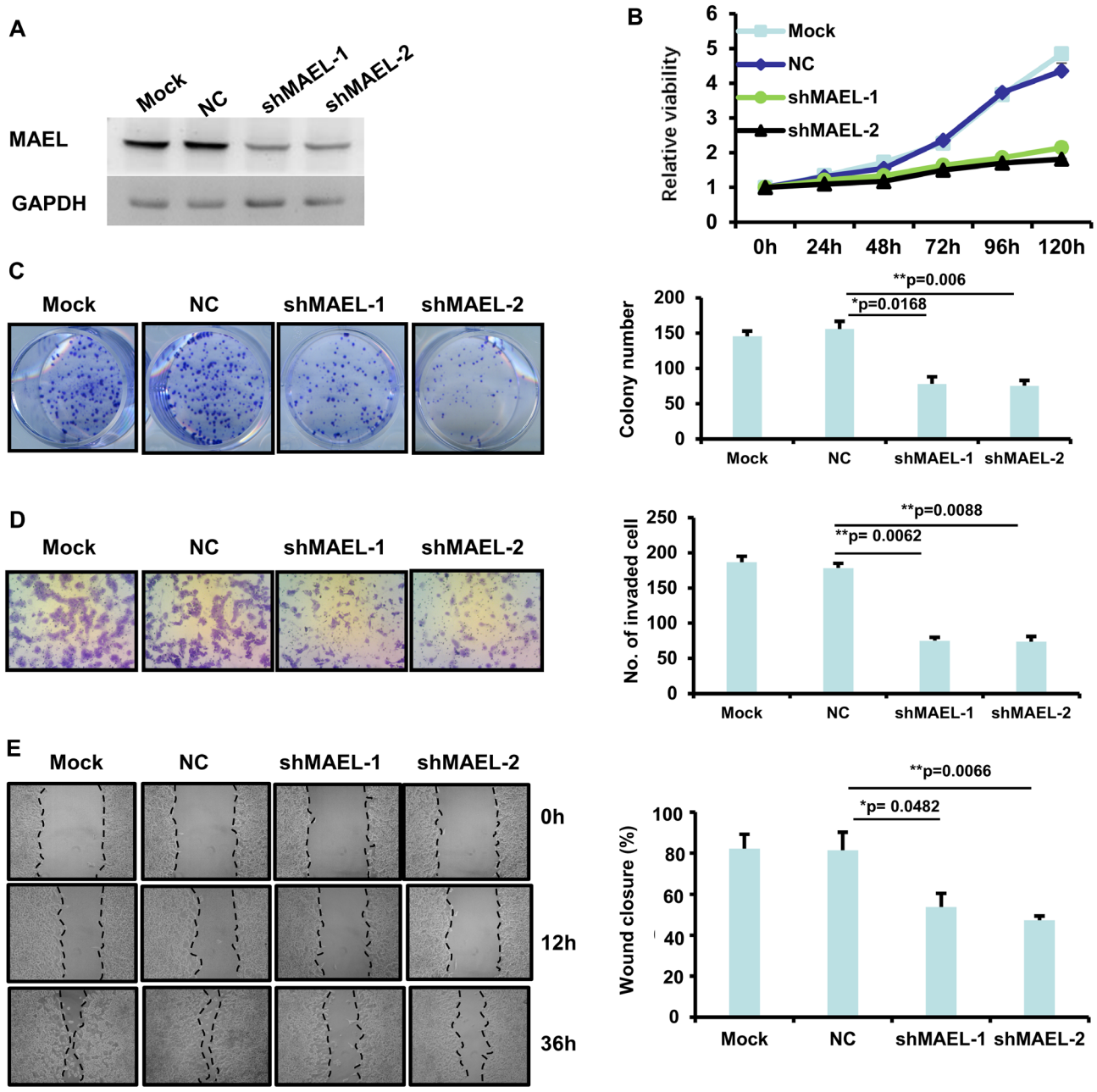

Supplementary Figure 3: *MAEL* knockdown inhibits proliferation, migration and invasion in SUN-1 cells. (**A**) MAEL protein levels in the untreated SUN-1 cells (mock) and the SUN-1 cells stably expressing *MAEL* shRNA (shRNA-1, shRNA-2) or scrambled shRNA (NC). (**B**) The cell growth was determined by MTT assay. (**C**) Representative images of colony (left panel) and the colony numbers (right panel). (**D**) Representative images (left panel) and statistical analysis (right panel) of invaded cells in the Transwell invasion assay. (**E**) Representative images of wound area (left panel) at the indicated time and percentage of wound closure (right panel) at 36 h after scratching. The target sequences of MAEL for constructing lentiviral shRNA were as follows: shRNA1: 5′-GGAACTGGCCACCTATCTACT-3′; shRNA2: 5′-GAGTCAACTGGTGTTTGAAGC-3′. All the values were presented as means ± S.D for at least three independent *in vitro* experiments. Differences between two groups were analyzed by student *t*-test; $^{*}p$-value ≤ 0.05 and $^{**}p$-value ≤ 0.01.

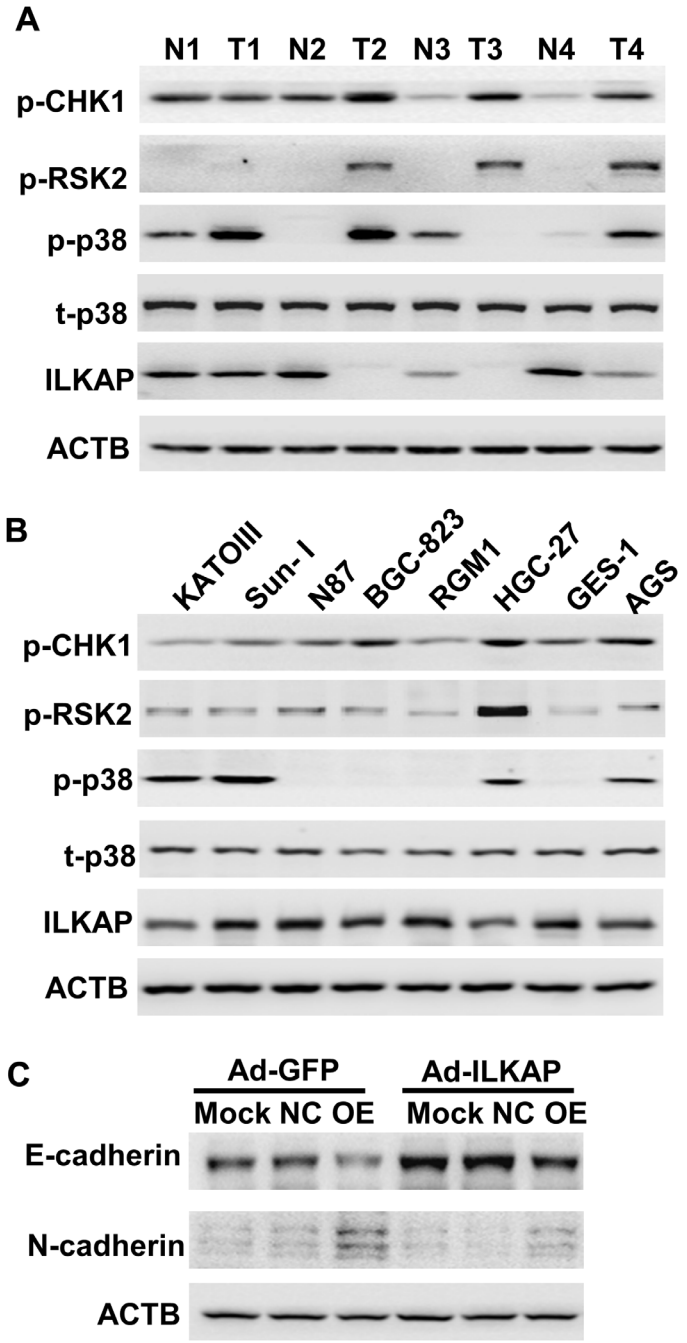

Supplementary Figure 4: Western blot analysis. (**A**) The expression of ILKAP and phosphorylated CHK1, RSK2, p38 in the 4 pairs of gastric tumor and adjacent normal tissues. (**B**) The expression of ILKAP protein and phosphorylated CHK1, RSK2, p38 in the gastric cell lines. (**C**) Effect of adenovirus-mediated ILKAP expression on the levels of E-cadherin and N-cadherin. The GES-1 cells (mock) and the GES-1 cells stably expressing empty vector (NC) or MAEL cDNA (OE) were infected with adenovirus expressing *GFP* or *ILKAP.* At 48 h after infection, the cells were harvested and subjected to Western blotting with indicated antibodies.

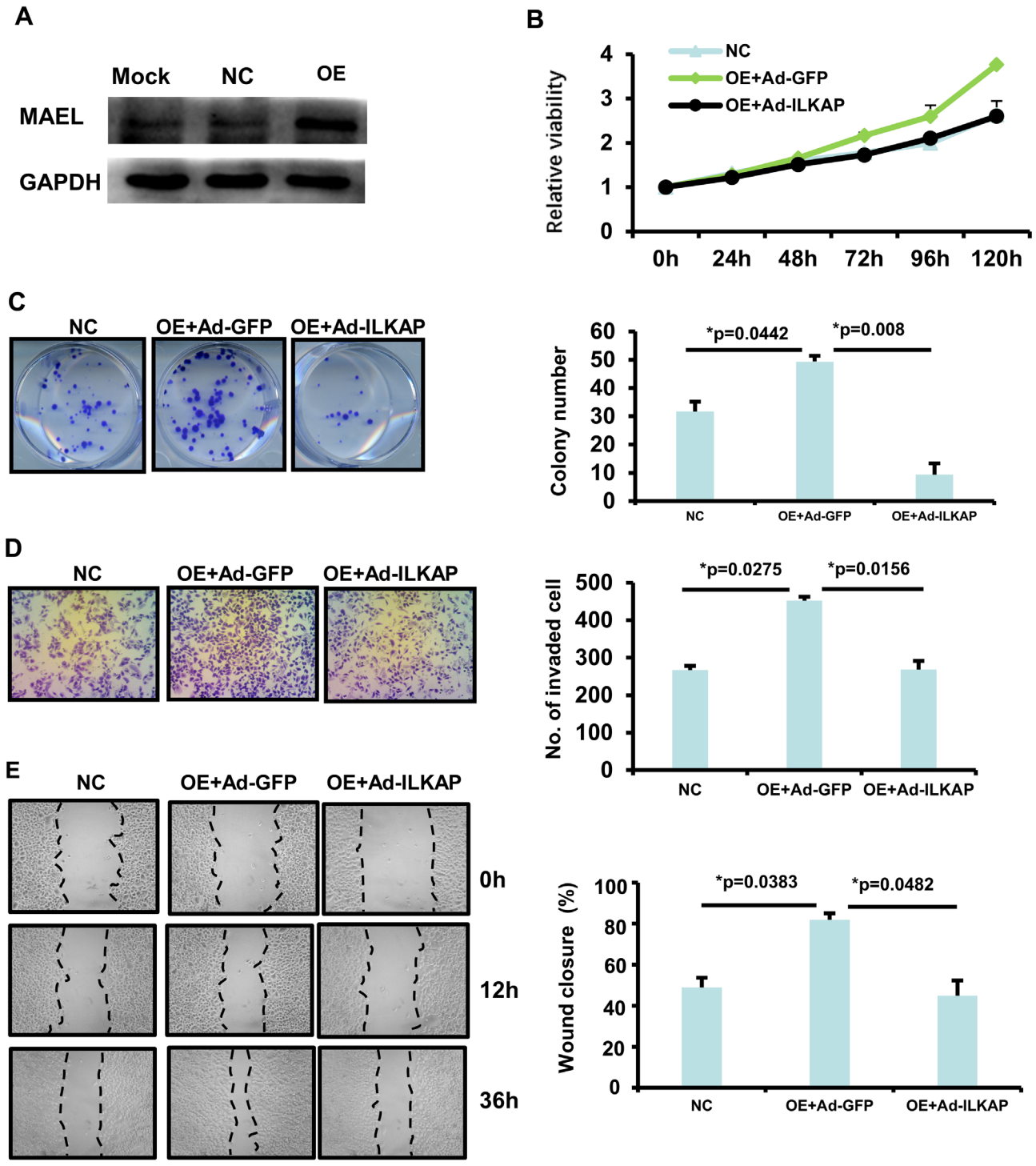

Supplementary Figure 5: Adenovirus-mediated *ILKAP* overexpression suppresses the oncogenic roles of *MAEL*. The BGC-823 cells stably expressing *MAEL* cDNA or empty vector were infected with adenovirus expressing GFP (Ad-GFP) or ILKAP (Ad-ILKAP). (**A**) The *MAEL* expression levels in BGC-823 cells (Mock) and the BGC-823 cells with stable expression empty vector (NC) or *MAEL* cDNA (OE) were detected by Western blotting. (**B**) Dynamic changes of cell viability determined by MTT assay. The cells were harvested for MTT assay at different time after adenovirus infection. (**C**) Representative images of colony (left panel) and the colony numbers (right panel). (**D**) Representative images (left panel) and statistical analysis (right panel) of invaded cells in the Transwell invasion assay. (**E**) Representative images (left panel) of wound area at the indicated time and percentage of wound closure at 36 h after scratching (right panel). All the values were presented as means ± S.D for at least three independent *in vitro* experiments. Differences between two groups were analyzed by student *t*-test; $^{*}p$-value ≤ 0.05 and $^{**}p$-value ≤ 0.01.

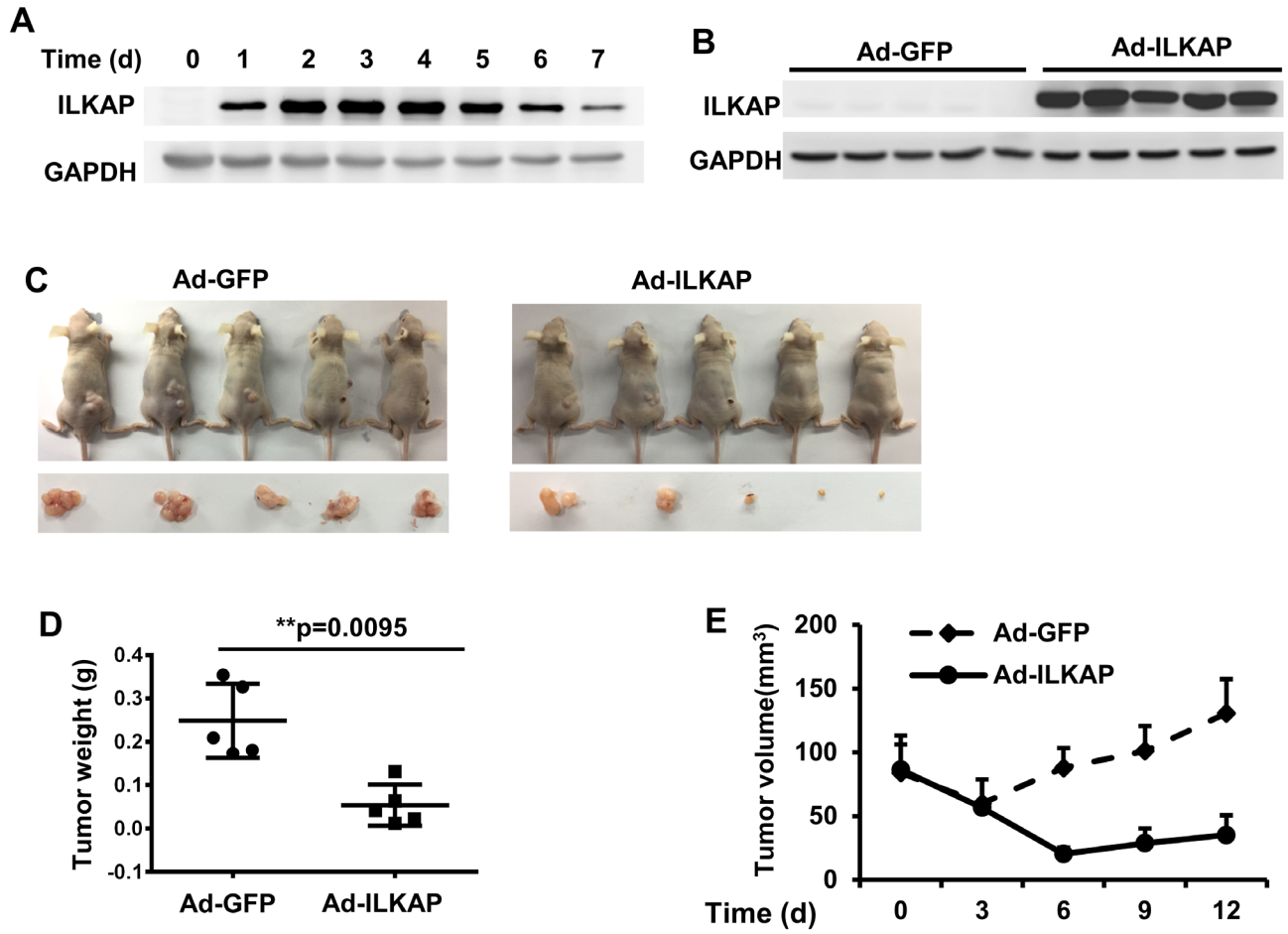

Supplementary Figure 6: Therapeutic effects of adenoviruses expressing ILKAP on xenograft tumors. (**A**) Dynamic changes of ILKAP protein levels in the HGC-27 cells after infection with adenoviruses expressing *ILKAP*. (**B**–**D**) The therapeutic effects of adenovirus-mediated ILKAP expression. BALB/c nude mice (7–8 weeks old) were injected with 5×10^6 HGC-27 cells at the back of nude mice. When the tumor volume reached 50–100 mm^3, the adenovirus expressing *ILKAP* or *GFP* were injected intratumorally at a dose of 1×10^9 PFU (pore-forming unit) in 100 μL of phosphate-buffered saline (PBS). Mice received a second injection at 2 days after the first injection. (**B**) Expression of ILKAP protein in the xenograft tumors injected with Ad-GFP or Ad-ILKAP at 48 h after injection. (**C**) Representative images of the xenograft tumors derived from HGC-27 cells at 15 days after adenovirus injection. (**D**) Weights of xenograft tumors at 15 days after adenovirus injection. (**E**) Dynamic volume of xenograft tumors at different time after adenovirus injection.

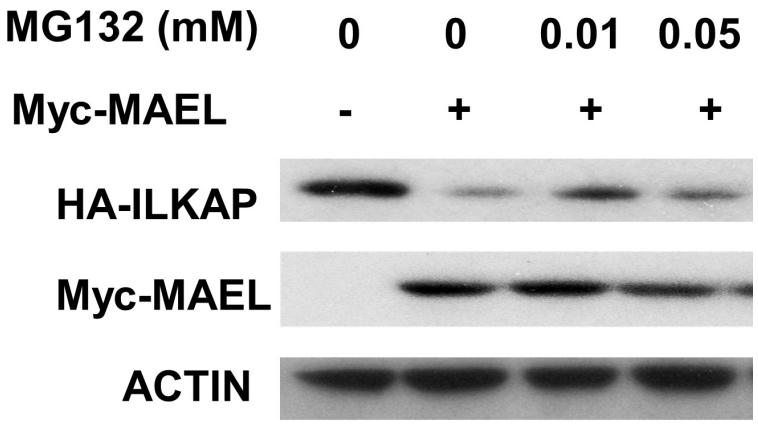

Supplementary Figure 7: Treatment with MG132 has no significant effect on ILKAP levels. The HEK293 cells were transfected with HA-ILKAP and Myc-MAEL plasmids and treated with CHX plus MG132 for 4 h, HA-ILKAP protein levels were detected by Western blotting.